LVRT Operation Enhancement of Single-Stage Photovoltaic Power Plants

An Analytical Approach

Nasiri, Mojtaba; Arzani, Ali; Guerrero, Josep M.

Published in:
IEEE Transactions on Smart Grid

DOI (link to publication from Publisher):
10.1109/TSG.2021.3108391

Publication date:
2021

Document Version
Accepted author manuscript, peer reviewed version

This article has been accepted for publication in a future issue of this journal, but has not been fully edited. Content may change prior to final publication. Citation information: DOI 10.1109/TSG.2021.3108391, IEEE Transactions on Smart Grid

LVRT Operation Enhancement of Single-Stage Photovoltaic Power Plants: An Analytical Approach

Mojtaba Nasiri, Ali Arzani, *Member, IEEE*, and Josep M. Guerrero, *Fellow, IEEE*

***Abstract*—The impact of grid-connected PV power plants (GCPPP) operation on the grid entails mandatory provision and conformable execution of futuristic grid-codes (GC) by GCPPP stakeholders. While standard GC-compliant reactive power injection occurs in the advent of voltage drops at the point of common coupling (PCC), weather-dependent active power delivery should also coincide. Hence, it is essential to derive the PV inverter current reference set-points meticulously and confine its current range. This paper proposes a novel control strategy for realization of enhanced LVRT operation in three-phase single-stage GCPPPs. The control scheme encompasses the following features: (a) PCC negative-sequence current reference set-points determination from its positive-sequence counterpart; as well as the analytical determination of PCC voltage sequence components, (b) GC-compliant reactive power injection, without causing second-order harmonic oscillations in the delivered active power to the grid during asymmetrical PCC faults, (c) utilization of a current limiter for immaculate regulation of the PV array output power. Simulation results reflect on the developed control scheme's effectiveness in significantly improving GCPPP LVRT operation for a wide range of operating conditions.**

***Index Terms*—Current limiter, grid-code, grid-connected photovoltaic power plant, low voltage ride-through**

NOMENCLATURE

Abbreviations

GC	grid-code
GCPPP	grid-connected photovoltaic power plant
InC	incremental conductance
LVRT	low voltage ride-through
MAF	moving average filters
MPP	maximum power point
MPPT	maximum power point tracking
PI	proportional-integral
PCC	point of common coupling
PLL	phase-locked loop
PV	photovoltaics
PV-VSC	PV inverter
PWM	pulsewidth modulation
SRF	dq-synchronous reference frame
STC	standard testing conditions
VSC	voltage source converter
VUF	unbalanced voltage factor

Subscripts

lim	limit
max	maximum
pu	per-unit
dq	direct & quadrature components in SRF
$c2$	cosine term
$s2$	sine term
f	filter and grid
0	average

Superscripts

$\pm$	positive- and negative-sequence
nom	nominal
ref	reference

Variables and Symbols

A	ideality factor
N_s	number of series panels
N_p	number of parallel panels
R_s	series resistance of the panel [Ω]
R_{sh}	shunt resistance of the panel [Ω]
V_{dc}	array terminal voltage [V]
I_{dc1}	PV array output current [A]
I_{dc2}	dc-current flowing into DC terminal of VSC [A]
C_{dc}	dc-link capacitance [F]
P_{grid}	injected active power to the grid [W]
e_{dqf}, v_{dqf}	GSC and PCC voltages in SRF [V]
i_{dqf}	injected current into the grid in SRF [A]
ω_f	grid voltage angular frequency [$\frac{\text{rad}}{\text{s}}$]
R_f, L_f	grid filter resistance [Ω] and inductance [H]
m	unbalanced voltage factor
$p.u.$	per-unit
P_{mp}	power at MPP [W]
V_{mp}	voltage at MPP [V]
I_{mp}	current at MPP [A]
V_{oc}	open circuit voltage [V]
I_{sc}	short circuit current [A]
α_i	temperature coefficient of I_{sh}
α_v	temperature coefficient of V_{oc}
P_{PV}	PV array output power [W]
I_n	VSC nominal current [A]
α	ratio between injected reactive current and VSC nominal output current
γ	adjustment coefficient for q-axis reference current set-point
ζ	coefficient, $i^{+}_{df-\text{lim}}$ relative to $I_{\max}$

Mojtaba Nasiri is a Research Fellow with the Solar Energy Applications Group, School of Engineering, Trinity College Dublin, Dublin 2, Ireland (e-mail: nasirim@tcd.ie).

Ali Arzani is a Research Assistant Professor with the Center for Energy Systems Research, Tennessee Technological University, Cookeville, TN 38505, USA (e-mail: aarzani@tntech.edu).

Josep M. Guerrero is a Professor with the Department of Energy Technology, Aalborg University, DK 9220, Denmark (e-mail: joz@et.aau.dk).

I. Introduction

Nowadays, standard grid-codes (GC) mandate grid-connected photovoltaic power plants (GCPPP) to perform grid-supporting functionalities in response to grid-faults and dependent on the fault type and severity at point of common coupling (PCC). Despite progressions in fully complying with the GCs, utilities, and GCPPP stakeholders are still facing multiple open challenges that impose adverse implications on GCPPP and grid operations. In addition to maintaining grid-connectivity and reactive current injection by the PV plant, the two significant challenges are (a) active power injection at PCC during a fault and post-fault clearance, (b) strategies to deal with oscillatory dc-link voltage waveforms with twice the grid frequency, that occur during asymmetrical grid-faults [1].

Grid-integration of a three-phase PV system takes place through either one or two power-processing stages [2], [3]. In a single-stage PV system, a three-phase dc-ac converter (PV-VSC) connects the PV array to the grid, while simultaneously keeping track of the maximum power point, i.e., MPPT by regulating the voltage across its dc-link capacitor (Fig. 1). In the event of a voltage drop at PCC, unlike a two-stage structure, the single-stage GCPPP does not encounter excessive voltage increase across its dc-link capacitor. In fact, as the dc-link voltage rises, the voltage across the PV array and its forming PV panels increases, forcing the operating point to automatically move to a new equilibrium and thus produce a lower amount of power [4]. Nevertheless, determination of a new operating point is always a challenge with single-stage GCPPPs. On the other hand, the PV array operation can be disrupted during asymmetrical faults. This is due to voltage oscillations with twice the grid frequency originating across the dc-link capacitor of a single-stage GCPPP. Generally, any form of disturbance in the grid can directly lead to undesirable implications on the performance of the PV array. In summary, the main challenges associated with operating single-stage GCPPP during voltage drops at PCC are as follows:

- PV array operating point moving further away from the MPP and post-fault clearance PV active power decrease, thus increasing the probability of instability in GCPPP operation. It is noteworthy that, GC recommends active power injection into PCC (subject to availability) during a voltage drop. However, a reduction in PV active power output is perceivable in circumstances where solar irradiance decreases [5].
- GC execution in injecting reactive current into PCC, while allocating the rest of the PV-VSC current capacity for active current injection (PV array production capacity) during various symmetrical and asymmetrical fault types.

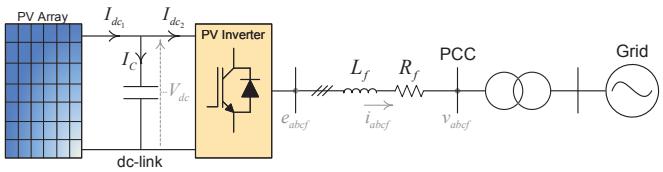

Fig. 1. Single-line diagram of a three-phase single-stage GCPPP

- Oscillations originating with two-times the grid frequency across the dc-link and PV array output during asymmetrical grid-side faults.
- Incapability of some of the PV-VSC controllers in handling negative-sequence effects appearing on the AC-side of the GCPPP during asymmetrical faults. This can lead to over-current in some phases or harmonics presence in the delivered current due to lack of effective current limiters during asymmetrical faults.

Hence, studies have been carried out in the past to resolve the issues mentioned earlier; some of which are briefly described in this section. Authors in [6] discuss controlling the positive-sequence current during asymmetrical faults. While simple and easy to operate, this type of control demonstrates a poor performance during asymmetrical voltage drops. This is due to a lack of control over the negative-sequence current. A controller is designed in [7] to ensure peak current limitation; however, with the drawback of current harmonics injection. Deployment of constant current limiters and lack of attention to the negative-sequence component during asymmetrical grid faults cause current harmonics. In [8], two limitations have been investigated supporting the grid voltage, i.e., current amplitude limit and the grid impedance limit. However, there is no discussion on the amount of PV array active power injection and the necessary limitations for it. In [9], several target functions are conceived, simultaneously. In this reference, three conditions have been considered: sole active power injection, simultaneous active and reactive power injection, and sole reactive power injection. One of the shortcomings of this research is the determination of the q-axis current limiter values (which is responsible for injecting reactive current into the PCC), which causes oscillations in the active output power. These oscillations may have adverse implications on the dc-link capacitor and PV array active power production.

In retrospect to PV array active power output generation and control, authors in [4] control the DC-DC converter duty-cycle to adjust the dc-link voltage. In some articles, such as [10], an inverter has been designed that not only reduces switching losses but also increases the converter's ability to inject reactive power into the grid to improve grid stability as well as LVRT. In this system, the PV array active power output is determined by regulating the dc-link voltage. However, there is a lack of research in linking the grid-side voltage drop condition to the determination of the PV array operating point. In [11], the moving average filters (MAF) technique has been developed to eliminate second-order harmonic oscillations during asymmetrical faults at PCC. This enhances active power and grid-side current waveforms. The main problem with this technique is the determination of dq-axes current reference set-points for the PV-VSC current controller during PCC fault events. This becomes much more complicated and cumbersome in the case of asymmetrical faults. In [12], an active power limitation scheme as well as a method for reactive power reference set-point calculation is proposed for the grid-side converter of a PMSG-based wind turbine. This is operational under different fault types and can be similarly integrated into the single-stage GCPPP's control

system with proper adjustments being applied. The salient features of this paper are as follows:

- An analytical approach for the determination of negative-sequence current amplitude that is required for grid-injection in order to avoid second-order harmonic oscillations in the injected active power into the grid at all operating modes and solely by having the d-axis positive-sequence current reference set-point. Utilizing current reference set-points resolves the issue in [9].
- Classification of the operating modes and regulation of the active power output of the PV array, taking into account the voltage drop condition at PCC. In fact, by modifying the PV array MPPT controller and also regulating the d-axis positive-sequence current per the GC reactive current injection requirements, maximum active power delivery to the grid is attained.
- Intact execution of GC-compliant reactive current delivery during voltage drops at PCC. This has been accomplished by the analytical determination of PV-VSC reactive current reference set-points for various types of faults.
- Implementation of a dual current controller for injecting negative-sequence current. Furthermore, the proposition and utilization of current limiters for over-current prevention.

II. Single-Stage PV Power Plant Grid Integration

Illustrated with Fig. 1, a single-stage GCPPP is composed of several components. A series-parallel combination of PV panels forming the plant's PV array, that produces variable DC power at its output terminals. The power conditioning unit comprises of the PV-VSC and its associated dc-link capacitor. Depending on system requirements, the PV-VSC delivers GC-compliant active and/or reactive current to the network after passing through a passive filter and a transformer. It also performs MPPT through proper regulation of the dc-link voltage. The governing equations of the single-stage GCPPP are presented for the PV-VSC as in (1)-(2) [13].

$$\frac{1}{2}C_{dc}\frac{dV_{dc}^2(t)}{dt} = P_{PV}(t) - P_{grid}(t) \tag{1}$$

$$\begin{cases} e_{dq}^{+} = R_f i_{dq}^{+} + L_f \dfrac{di_{dq}^{+}}{dt} + j\omega_f L_f i_{dq}^{+} + v_{dq}^{+} \\ e_{dq}^{-} = R_f i_{dq}^{-} + L_f \dfrac{di_{dq}^{-}}{dt} - j\omega_f L_f i_{dq}^{-} + v_{dq}^{-} \end{cases} \tag{2}$$

In the studies of this paper, the TOPSUN PV module has been utilized, with its specifications presented in the appendix. The GCPPP developed for this research is rated at $1.5MW_p$, $480V_{ac}$ at standard testing conditions (STC) of ($1000W/m^2$,25 °C) [13]. This entails a dc-link voltage over $800V$ that is achieved by connecting 17 PV modules in series. Each module corresponds to an MPP voltage and current of $(49.78V, 8.04A)$. To generate $1.5MW_p$, the PV array consists of 3740 modules leading to 220 PV strings in parallel to conform to the output current requirements of the GCPPP, i.e., $1768.8A$ at STC. Concerning the MPPT method, the common incremental conductance (InC) method has been incorporated.

The grid-side active and reactive powers are generally expressed as follows, taking into account voltage and current negative-sequence components [14], [15]

$$\begin{cases} P_{grid}(t) = P_0 + P_{c2}\cos(2\omega_f t) + P_{s2}\sin(2\omega_f t) \\ Q_{grid}(t) = Q_0 + Q_{c2}\cos(2\omega_f t) + Q_{s2}\sin(2\omega_f t) \end{cases} \tag{3}$$

where

$$\begin{cases} P_0 = \frac{3}{2} \times \left(v_{df}^{+} i_{df}^{+} + v_{qf}^{+} i_{qf}^{+} + v_{df}^{-} i_{df}^{-} + v_{qf}^{-} i_{qf}^{-} \right) \\ Q_0 = \frac{3}{2} \times \left(v_{qf}^{+} i_{df}^{+} - v_{df}^{+} i_{qf}^{+} + v_{qf}^{-} i_{df}^{-} - v_{df}^{-} i_{qf}^{-} \right) \end{cases} \tag{4}$$

$$\begin{cases} P_{c2} = \frac{3}{2} \left(v_{df}^{+} i_{df}^{-} + v_{qf}^{+} i_{qf}^{-} + v_{df}^{-} i_{df}^{+} + v_{qf}^{-} i_{qf}^{+} \right) \\ P_{s2} = \frac{3}{2} \left(v_{df}^{-} i_{df}^{+} - v_{qf}^{-} i_{qf}^{+} - v_{df}^{+} i_{df}^{-} + v_{qf}^{+} i_{qf}^{-} \right) \end{cases} \tag{5}$$

III. Control Circuit Design & PV-VSC Proposed LVRT Scheme

In this section, controller design objectives and its analytical formulation are presented.

A. Control Objectives

The major novelty of this research leading to LVRT operation enhancement of GCPPPs during voltage drops originates from the concurrent implementation of the control objectives. These objectives are:

a) Implementation of GC-compliant positive-sequence reactive current injection, taking into account the absence of active power oscillations in all operation modes during asymmetrical faults.

b) Confinement of all phase currents amplitude delivered to the network. This is achieved for all fault types, i.e., symmetrical and asymmetrical; and even for deep voltage drops.

c) PV array maximum active power injection in accordance with the GC requirement and converter current capacity.

d) Preventing P_{grid} and V_{dc} second-order harmonic oscillations during asymmetrical faults through implementation of dual current control and determination of current limiters set-points compatible with asymmetrical faults.

B. Reactive Current Reference Set-Point ($i_{qf}^{+\,\mathrm{ref}}$)

Calculating the reactive current reference ($i_{qf}^{+\,\mathrm{ref}}$) according to the GC, plays a crucial role in achieving the intended control objectives during symmetrical and asymmetrical voltage drops. In the Danish GC for reactive current injection, a GCPPP is required to inject positive-sequence current according to the following expression [16].

$$\alpha = \frac{\left|i_{qf}^{+}\right|}{I_{\max}} = \begin{cases} 0 & v_{df-pu}^{+} \geq 0.9 \\ -2.5v_{df-pu}^{+} + 2.25 & 0.5 \leq v_{df-pu}^{+} < 0.9 \\ 1 & v_{df-pu}^{+} < 0.5 \end{cases} \tag{6}$$

However, due to the presence of a negative-sequence voltage during asymmetrical faults, oscillations with twice the grid frequency occur in the active and reactive power delivered to the network (3) [17]. On the other hand, the presence of a negative-sequence voltage affects P_0 and Q_0 values. In

This article has been accepted for publication in a future issue of this journal, but has not been fully edited. Content may change prior to final publication. Citation information: DOI 10.1109/TSG.2021.3108391, IEEE Transactions on Smart Grid

fact, with a dual current controller being utilized, negative-sequence current becomes present according to (4). Hence, considering the negative-sequence in determining the positive-sequence active- and reactive-current reference set-points plays an integral role in the amount and quality of the deliverable power to the network. To account for this phenomenon in analytical formulations, a factor called the unbalanced voltage factor (VUF) is defined [18], as shown in this article with m.

$$m = VUF = \frac{\left| v_{dqf}^{-} \right|}{\left| v_{dqf}^{+} \right|} \tag{7}$$

where $\left| v_{dqf}^{+} \right| = \sqrt{{v_{df}^{+}}^2 + {v_{qf}^{+}}^2}$, $\left| v_{dqf}^{-} \right| = \sqrt{{v_{df}^{-}}^2 + {v_{qf}^{-}}^2}$. In contrary to [9], in this paper the effect of m in determining $i_{qf}^{+\,\mathrm{ref}}$ during asymmetrical faults has been considered. As a result, $i_{qf}^{+\,\mathrm{ref}}$ is defined from [6], as follows

$$i_{qf}^{+\,\mathrm{ref}} = -\gamma \alpha I_{\max} \tag{8}$$

The γ value that is the adjustment coefficient for the q-axis reference current set-point depends on m and the extent of the voltage drop, and is calculated in the following subsection.

C. Active Current Reference Set-Point and Current Limitation Scheme ($i_{df}^{+\,\mathrm{ref}}$)

One must consider two points when determining the reference set-point and d-axis positive-sequence current limiter: (a) the range of the phases' injected current at PCC is limited, and (b) reactive current injection in accordance with (8). Hence, the following control objective must be achieved

$$\max\{I_a, I_b, I_c\} \le I_{\max} \tag{9}$$

subject to (8). On the other hand, (9) can be rewritten as follows in the SRF

$$\left| i_{dqf}^{+} \right| + \left| i_{dqf}^{-} \right| \le I_{\max} \tag{10}$$

where $\left| i_{dqf}^{+} \right| = \sqrt{{i_{df}^{+}}^2 + {i_{qf}^{+}}^2}$, $\left| i_{dqf}^{-} \right| = \sqrt{{i_{df}^{-}}^2 + {i_{qf}^{-}}^2}$.

Since the positive-sequence vector of the PCC voltage is aligned with the d-axis in the SRF, voltage's positive-sequence vector projected on the q-axis v_{qf}^{+}=0. Thus, (7) is rewritten as follows

$$m = \frac{\sqrt{{v_{df}^{-}}^2 + {v_{qf}^{-}}^2}}{\left| v_{df}^{+} \right|} \tag{11}$$

By definition, (12) holds and substituting them in (11) followed by a power of two, yields (13).

$$m_d = \frac{\left| v_{df}^{-} \right|}{\left| v_{df}^{+} \right|} \ , \ m_q = \frac{\left| v_{qf}^{-} \right|}{\left| v_{df}^{+} \right|} \tag{12}$$

$$m^2 = m_d^2 + m_q^2 \tag{13}$$

The PV-VSC controller must also generate a negative-sequence current to overcome the second-order oscillations of the active power. Therefore, the ratio of the negative current to the positive-sequence amplitude should be equal to m.

$$m = \frac{\left| i_{dqf}^{-} \right|}{\left| i_{dqf}^{+} \right|} \tag{14}$$

Now, according to (10) and (14), one can derive (15), and from squaring the two sides of the resulting expression and incorporating (8) yields (16).

$$(1+m)\left| i_{dqf}^{+} \right| \le I_{\max} \tag{15}$$

$${i_{df}^{+}}^2 + \gamma^2 \alpha^2 I_{\max}^2 \le \frac{I_{\max}^2}{(1+m)^2} \tag{16}$$

By simplifying and subtracting from (16) as well as placing $i_{df-\lim}^{+}$ in place i_{df}^{+}, a high limit of positive d-axis sequence current is obtained

$$i_{df-\lim}^{+} = I_{\max}\sqrt{\frac{1-\gamma^2\alpha^2(1+m)^2}{(1+m)^2}} = \zeta I_{\max} \tag{17}$$

Where ζ is $i_{df-\lim}^{+}$ relative to $I_{\max}$, and the γ value is

$$\gamma = \begin{cases} 1 & 1 \ge \alpha(1+m) \\ \frac{1}{\alpha(1+m)} & 1 < \alpha(1+m) \end{cases} \tag{18}$$

To examine the limitations in the calculation of $i_{qf}^{+\,\mathrm{ref}}$ and the value of $i_{df-\lim}^{+}$ in $pu.$, Figs. $2(a,b)$ are depicted. As shown in Fig. $2c$, according to (8) the $\left| i_{qf}^{+\,\mathrm{ref}} \right|$ decreases with increasing m. This decrease in $\left| i_{qf}^{+} \right|$ is due to the ability to inject dq-axes negative-sequence currents. Because if the total capacity of the converter is allocated to $\left| i_{qf}^{+} \right|$ injection, according to (5), the components P_{c2}=P_{s2}=0 will not be (explanations will be provided in Section III.D). It should be noted that in asymmetrical faults, the utility must either accept the injection of a positive q-axis sequence current with full capacity or inject the active power without second-order harmonic oscillations. Therefore, it seems that in PV systems whose converter is equipped with a negative-sequence injection controller, it is better to apply a $\left| i_{qf}^{+\,\mathrm{ref}} \right|$ restriction to inject a negative-sequence current so that both active-power delivered and V_{dc} become without second-order harmonic oscillations. This eliminates ripples across the PV array operating point, preventing dc-link capacitor from becoming damaged. Fig. $2c$ shows how γ varies with respect to m and $\left| v_{df}^{+} \right|$. As can be seen, in the case of deep asymmetric

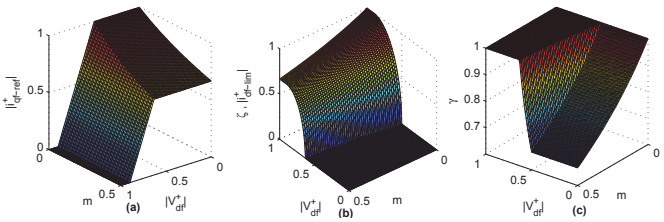

Fig. 2. **(a)** $i_{qf}^{+\,\mathrm{ref}}$ based on (m, v_{df}^{+}), **(b)** $(\zeta, i_{df-\lim}^{+})$ based on (m, v_{df}^{+}), and **(c)** γ based on (m, v_{df}^{+})

This article has been accepted for publication in a future issue of this journal, but has not been fully edited. Content may change prior to final publication. Citation information: DOI 10.1109/TSG.2021.3108391, IEEE Transactions on Smart Grid

voltages, the γ value will be less than 1. Fig. $2b$ shows the value of $i^{+}_{df-\lim}$ and ζ with respect to m and $\left|v^{+}_{df}\right|$. At voltage drops of more than 50%, regardless of whether the voltage drop is symmetrical or asymmetrical, the value of $i^{+}_{df-\lim}$ must be zero. During asymmetrical voltage drops, its value in voltage drops below 50% is also zero, reckoning that the whole VSC capacity is allocated to reactive current injection.

D. Negative-Sequence Currents Reference Set-points ($i^{-\,\text{ref}}_{dqf}$)

As mentioned earlier, to preclude second-order harmonic oscillations from active power and V_{dc} waveforms during asymmetrical faults, a dual-current control strategy, is recommended. Its control target is to reach P_{c2}=P_{s2}=0. Therefore, using (4), (5) and considering P_{c2}=P_{s2}=0, the dq-axes currents' negative sequence component can be obtained as a function of positive sequence currents

$$i^{-}_{df} = \frac{1}{{v^{+}_{df}}^{2} + {v^{+}_{qf}}^{2}} \begin{bmatrix} i^{+}_{df}(v^{-}_{qf}v^{+}_{qf} - v^{-}_{df}v^{+}_{df}) \\ \\ + \, i^{+}_{qf}(-v^{-}_{qf}v^{+}_{df} - v^{-}_{df}v^{+}_{qf}) \end{bmatrix} \tag{19}$$

$$i^{-}_{qf} = \frac{1}{{v^{+}_{df}}^{2} + {v^{+}_{qf}}^{2}} \begin{bmatrix} i^{+}_{df}(-v^{-}_{qf}v^{+}_{df} - v^{-}_{df}v^{+}_{qf}) \\ \\ + \, i^{+}_{qf}(-v^{-}_{qf}v^{+}_{qf} + v^{-}_{df}v^{+}_{df}) \end{bmatrix} \tag{20}$$

Possessing $i^{+\,\text{ref}}_{df}$, $i^{+\,\text{ref}}_{qf}$ values and substituting in (19) and (20), the negative-sequence currents' reference set-points can be obtained. If v^{+}_{qf}=0, then (19) and (20) are simplified to

$$i^{-\,\text{ref}}_{df} = -\left(m_d i^{+\,\text{ref}}_{df} + m_q i^{+\,\text{ref}}_{qf}\right) \tag{21}$$

$$i^{-\,\text{ref}}_{qf} = m_d i^{+\,\text{ref}}_{qf} - m_q i^{+\,\text{ref}}_{df} \tag{22}$$

In the above expressions, values of $i^{+\,\text{ref}}_{qf}$ and $i^{+\,\text{ref}}_{df}$ are obtained from (8) and Fig. $3d$, respectively.

Figs. 3 and 4 show the block diagram of the PV-VSC controller and its operational flowchart, respectively. The calculation procedures for $i^{+\,\text{ref}}_{qf}$ and $i^{+}_{df-\lim}$ is displayed in Figs. $3(a-c)$. The three fundamental subdivisions of the control circuit is depicted in Fig. $3d$. In the first subdivision, the MPPT controller has been improved to keep constant V^{ref}_{dc} to its pre-fault value when $i^{+\,\text{ref}}_{df} \geq i^{+}_{df-\lim}$. By doing this, after the constraint $i^{+\,\text{ref}}_{df} \geq i^{+}_{df-\lim}$ has been removed, the PV array will be capable of performing MPPT in a faster manner. In the second subdivision, a comparison takes place between V_{dc} and V^{ref}_{dc} and then its difference fed into a PI controller to construct the d-axis reference current. When $i^{+\,\text{ref}}_{df} \geq i^{+}_{df-\lim}$, the d-axis reference current will become equal to $i^{+}_{df-\lim}$. Under this circumstance, the PI controller is equipped with an anti-windup system to increase the post-fault clearance [4]. Eventually, in the final subdivision, the dq-axes negative-sequence reference set-points are calculated using $i^{+\,\text{ref}}_{qf}$ and $i^{+\,\text{ref}}_{df}$ values. The significant point to perceive in Fig. $3c$ is that, when $i^{+\,\text{ref}}_{df} \geq i^{+}_{df-\lim}$ and the reference current set-point becomes equal to $i^{+}_{df-\lim}$, the PV array operating point will change (Section III.E). Fig. $3e$ illustrates the positive- and negative-sequence current controllers and the final phase of generating the switching pulses for the PV-VSC high-power semiconductor valves.

One can extract P_0 using (4), (21), (22), and with the assumption of the positive- and negative-sequence current components accurately tracking their corresponding current reference set-points

$$P_0 = \frac{3}{2}v^{+}_{df}\left(i^{+}_{df} + m_d i^{-}_{df} + m_q i^{-}_{qf}\right) = \frac{3}{2}v^{+}_{df}i^{+}_{df}\left(1 - m^2\right) \tag{23}$$

According to the above expression, during asymmetrical faults, the P_0 value decreases by the amount of m^2 compared to symmetrical faults. The rationale for this is the injection of negative-sequence currents for the execution of the control objective, i.e. P_{c2}=P_{s2}=0. The active-power limit injected at PCC can also be calculated from the following expression

$$P_{0-\lim} = \frac{3}{2}v^{+}_{df}i^{+}_{df-\lim}\left(1 - m^2\right) \tag{24}$$

E. DC-Link Voltage Reference Set-Point Calculation

As described earlier for Fig. $3c$, in the event of a PCC voltage drop, two cases may occur for the d-axis positive-sequence current reference set-point:
(a) $i^{+\,\text{ref}}_{df} < i^{+}_{df-\lim}$, (b) $i^{+\,\text{ref}}_{df} \geq i^{+}_{df-\lim}$

In case (a), the PV array continues tracking the MPP, since there is the VSC capability and capacity of current and active-power injection at PCC, for this case. Thus, the standard procedure is carried out for determining the PV power MPP.

In case (b), $i^{+\,\text{ref}}_{df}$ generated at the PI compensator output (Fig. $3c$) is greater than the calculated current limit from (17). Hence, the MPPT controller is disabled and the new operating point of the PV array is determined using $i^{+}_{df-\lim}$. According to Fig. 5, the PV array current moves from I_{mpp} to I_{LVRT} that corresponds to $i^{+}_{df-\lim}$. In this case, V_{dc} changes according to the new operating point V_{LVRT}, and the generation capacity will go down to P_{LVRT}. It should be noted that this change will always be to the right of the MPP; Since moving to the left of the curve to reduce generation capacity requires increasing PV current, that is not feasible. This brings numerous advantages such as ensuring PV array output current reduction, as well as ensuring power injection into the PCC by maintaining V_{dc} to a voltage higher than the PV-VSC dc-side requirement. This is because in a single-stage GCPPP, unlike the two-stage structure, there is no dc-dc converter for V_{dc} regulation.

IV. Results & Discussions

In this section, several simulations are performed in MATLAB/Simulink to evaluate the developed control system's performance for the GCPPP and the effectuality of the proposed LVRT operation strategy under specific operating conditions. The main specifications of the system are given in the Appendix. The time-domain simulations and analyses are framed under two scenarios: (a) symmetrical voltage drops, (b) asymmetrical voltage drops. To have a comprehensive evaluation, several solar irradiance and voltage drop perturbations have been applied in each scenario. The solar irradiance varies according to Fig. $6a$, where its set to $400W/m^2$ during $3 \leq t < 7$ and $1000W/m^2$ at other times. To facillitate the

This article has been accepted for publication in a future issue of this journal, but has not been fully edited. Content may change prior to final publication. Citation information: DOI 10.1109/TSG.2021.3108391, IEEE Transactions on Smart Grid

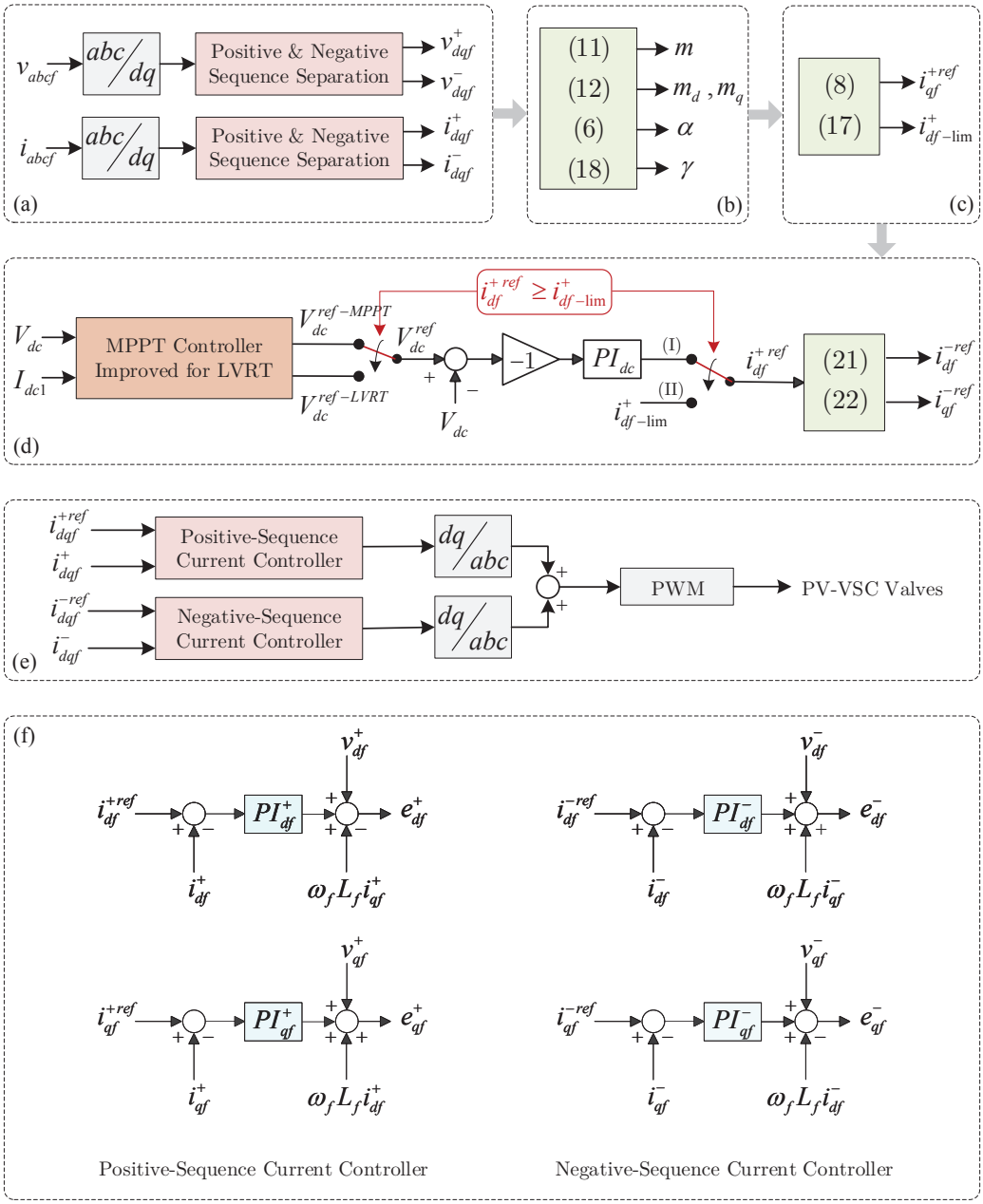

Fig. 3. Block diagram of the PV-VSC control structure comprising **(a)** PCC voltage/current sequence separations, **(b)** calculation of VUF and the limiters' coefficients, **(c)** calculation of reference set-points and positive sequence current limiter boundaries, **(d)** determination of $(i_{df}^{+\,\mathrm{ref}})$, dq-axes negative-sequence components, **(e)** determination of voltages reference set-points for the generation of PV-VSC switching pulses, and **(f)** closed-loop current controllers for positive and negative sequences

assessment, the operating points time-frames are identical for both scenarios and identified as

$$\begin{aligned}(0 \le t < 1 \ \ \& \ \ 9 \le t < 11) &\longmapsto \mathbf{O}\\ 1 \le t < 3 &\longmapsto \mathbf{A}\\ 3 \le t < 5 &\longmapsto \mathbf{B}\\ 5 \le t < 7 &\longmapsto \mathbf{C}\\ 7 \le t < 9 &\longmapsto \mathbf{D}\end{aligned}$$

A. Scenario 1: Symmetrical Voltage Drop

Two sequences of four-seconds long symmetrical voltage drops are applied at PCC, i.e., at t=1s and t=5s, respectively (Fig. 6b). The corresponding voltage magnitudes during A,B and C,D, reaches $0.15pu.$ and $0.65pu.$, respectively. Considering the voltage drop symmetry, its negative sequence component is zero and v_{df}^{+} is equivalent to the peak value of the PCC phase voltages. While coefficients α, γ, ζ are a function of voltage and type of fault on the grid-side; the voltage drops are similar during A,B and C,D. This leads to the coefficients carrying the same values during these two time intervals. Due to voltage drop symmetry, γ=1 in all the aforementioned time intervals. Given the depth of the voltage drop during A,B, the total PV-VSC capacity is devoted to injecting positive-sequence reactive current; conveying γ=0.

This article has been accepted for publication in a future issue of this journal, but has not been fully edited. Content may change prior to final publication. Citation information: DOI 10.1109/TSG.2021.3108391, IEEE Transactions on Smart Grid

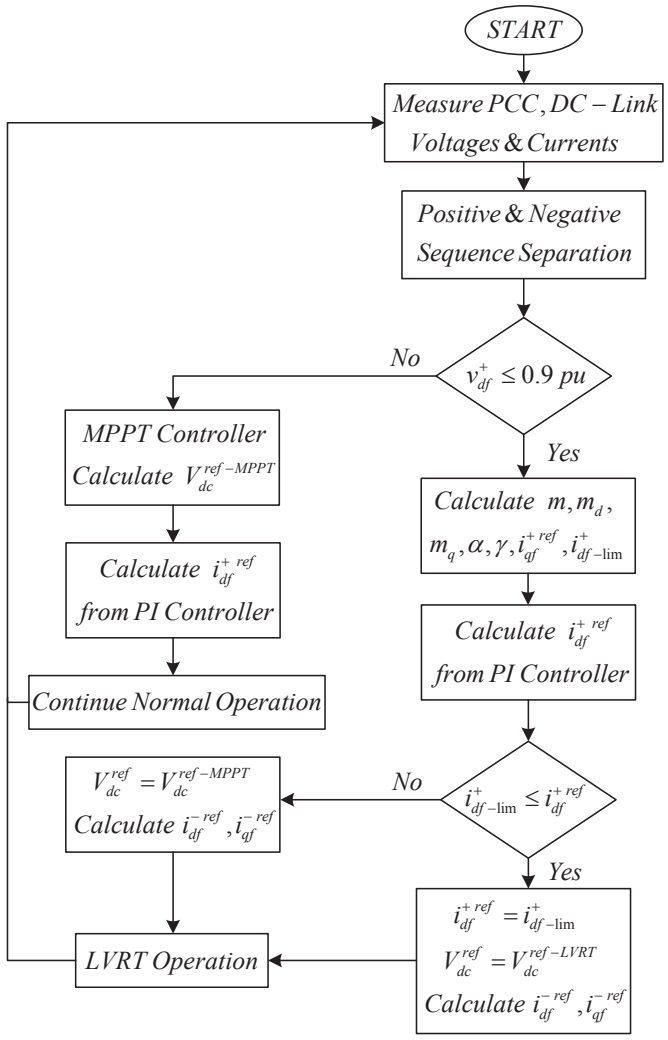

Fig. 4. Flowchart of the proposed control system

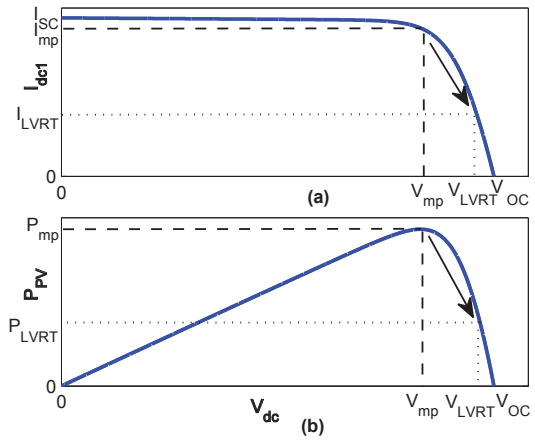

Fig. 5. PV array equilibrium operating point changes to reconcile the proposed LVRT operation strategy **(a)** $V_{dc} - I_{dc1}$ curve, **(b)** $V_{dc} - P_{PV}$ curve

Table I in the Appendix presents entire values of the parameters, currents, voltages, and resulting powers of all simulation studies. This helps to avoid mentioning each of corresponding values throughout the text. Hence, the simulations' waveforms will be discussed and analyzed in this section, exclusively.

Fig. 7a presents $\left|i_{qf}^{+}\right|$, i_{df}^{+}, and $i_{df-\lim}^{+}$ waveforms. As can be seen during A,B the entire capacity of the PV-VSC is allocated to current injection. In the C time interval, $i_{df-\lim}^{+}$ is greater than the current produced by the PV array. Thus, the array continues to generate its maximum power. In the D time interval, i_{df}^{+} must be confined by the current limiter due to the increase in solar irradiance. Fig. 7b shows the PV-VSC current injection into PCC. It can be observed that maximum current injection is well-confined at all time intervals.

Fig. 8a shows the V_{dc} waveform. It can be perceived from $i_{df}^{+\ \mathrm{ref}} \ge i_{df-\lim}^{+}$ during A,B and D, that V_{dc} is regulated according to the current limits, hence the voltage across the PV array increases. During time interval C, the PV array voltage is set based on the MPP. Figs. $8(b, c)$ show the waveforms of the active PV power generated and injected into the network as well as the reactive power.

In order to better investigate the process of active power regulation and PV array current generation at different operating conditions, i.e., grid voltage drops and PV solar irradiances,

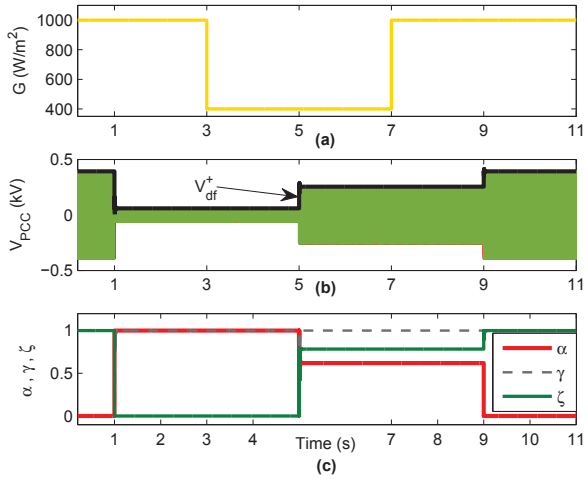

Fig. 6. Characteristics of **(a)** solar irradiance, **(b)** PCC voltage and v_{df}^{+} , and **(c)** α, γ, ζ

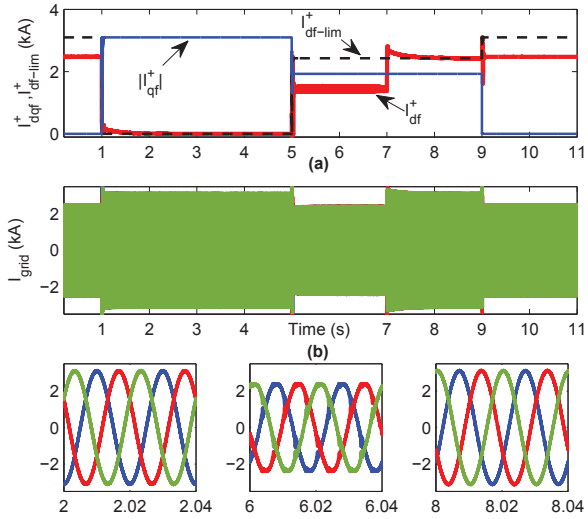

Fig. 7. Characteristics of **(a)** dq-axes positive-sequence current amplitudes, $i_{df-\lim}^{+}$, **(b)** PCC current waveforms in the proposed method

This article has been accepted for publication in a future issue of this journal, but has not been fully edited. Content may change prior to final publication. Citation information: DOI 10.1109/TSG.2021.3108391, IEEE Transactions on Smart Grid

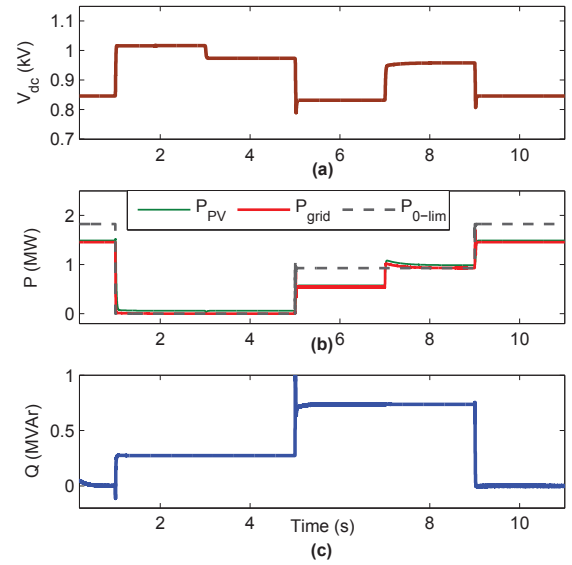

Fig. 8. Characteristics of **(a)** V_{dc}, **(b)** $(P_{PV}, P_{grid}, P_{0-\lim})$, and **(c)** Q

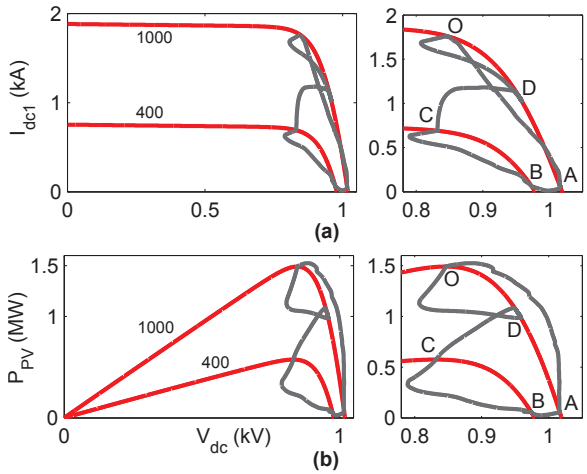

Fig. 9. PV array operating point alterations **(a)** $V_{dc} - I_{dc1}$ curve, **(b)** $V_{dc} - P_{PV}$ curve

Figs. $9(a, b)$ are presented. These figures depict the PV array operating point's moving trajectory, which changes based on the specified permissible active current. In the event of a deep voltage drop, the operating point moves down from point O to point A. Instead, if solar irradiance across the GCPPP varies at the same time the deep voltage drop occurs at PCC, the new equilibrium operating point will become point B. Subsequently, the PCC voltage increases to $0.65pu$. In this case the PV array is allowed to operate at MPP, i.e., the C time interval, due to the rise in PV-VSC current capacity. Then, solar irradiance increases to $1000W/m^2$, enforcing a new operating point, i.e., D, as the current reference set-point equals $i^+_{df-\lim}$ again. Eventually, with the fault clearance, the PV array operating point returns back to point O.

B. Scenario 2: Asymmetrical Voltage Drop

A two-phase to ground asymmetrical voltage drop is applied to PCC voltage phases bc (Fig. $10a$). The PCC voltage positive- and negative-sequence components are shown in Fig. $10b$. According to Fig. $10c$, γ=0.604 during A, B. This

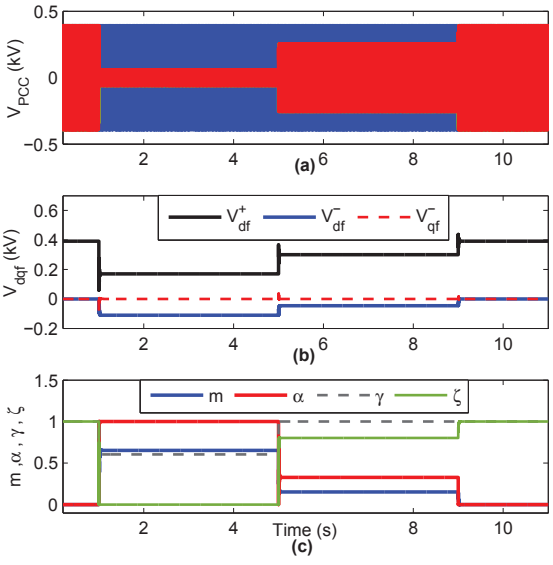

Fig. 10. Characteristics of **(a)** PCC voltage, **(b)** PCC voltage sequence components, and **(c)** m, α, γ, ζ

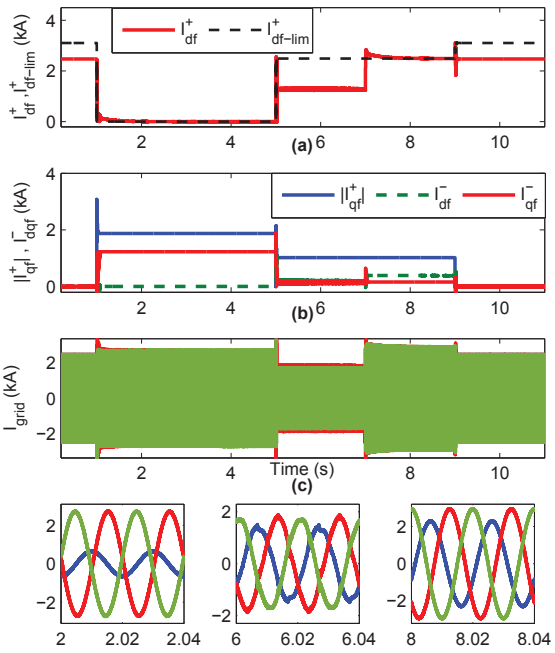

Fig. 11. Characteristics of **(a)** i^+_{df}, $i^+_{df-\lim}$ **(b)** i^-_{dqf}, i^+_{qf} and **(c)** PCC current

causes $i^{+\,\mathrm{ref}}_{qf}$ to become less than $I_{\max}$ and the remaining PV-VSC capacity utilized for negative-sequence current injection to prevent active power oscillations.

Fig. $11a$ depicts i^+_{df} and $i^+_{df-\lim}$ waveforms, while Fig. $11b$ exhibits $\left|i^+_{qf}\right|$ and axes' negative-sequence waveforms. Due to negative-sequence current injection mandate during A, B, $\left|i^+_{qf}\right| < I_{\max}$. Fig. $11c$ demonstrates current injection at PCC. As can be seen, all the phases' peak current is less than $I_{\max}$ at all time intervals.

Fig. $12a$ depicts the PV-VSC current space-vector trajectory, measured at PCC from t=0.2s to t=11s, while Fig. $12b$ enables improved visualization of this. The current in all intervals is less than the PV-VSC maximum current of $I_{\max}$=3.1kA,

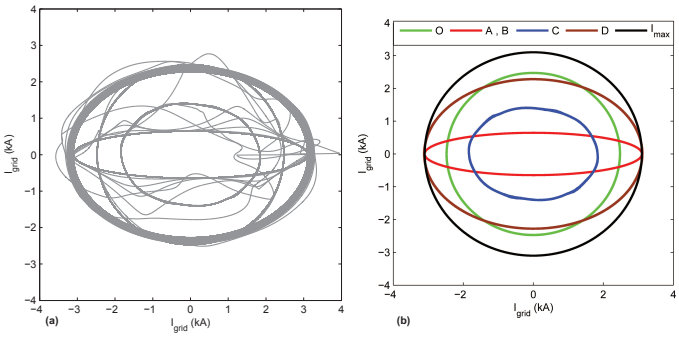

Fig. 12. Trajectory of PV-VSC current space-vector at its different operating points, demonstrating (a) transient conditions, (b) steady-state conditions

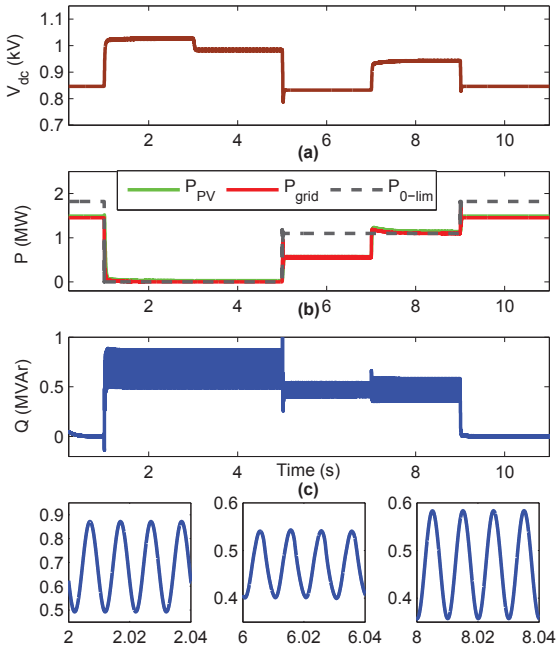

Fig. 13. Characteristics of **(a)** V_{dc}, **(b)** $(P_{PV}, P_{grid}, P_{0-\lim})$, and **(c)** Q

which confirms both the current limiter proper performance and the determined reference set-points of dq-axes positive- and negative-sequence currents.

According to Figs. $13(a,b)$, despite an asymmetrical grid fault, second-order harmonic oscillations are no longer visible in V_{dc}, P_{PV}, and P_{grid}. This is due to incorporation of a dual current controller and proposed current limiters. On the other hand, the power produced is lower than $P_{0-\lim}$ in all time intervals. Fig. $13c$ shows reactive power injection at PCC, which encompasses oscillations twice the grid frequency, inevitablely originating from fulfilling PV-VSC control objectives.

V. Conclusions

This paper proposes a novel control scheme for GCPPP LVRT operation enhancement, spanning the full range of operating modes. The results reflect on GCPPP resiliency during PCC faults, as well as its delay-free post-fault normal operation continuation, delivering active-power to the grid. A salient feature of this scheme discloses under deep and asymmetrical voltage drops at PCC, i.e., eliminating the second-order harmonic oscillations in the PV-VSC injected active power into the network; that is attained as a result of injecting a negative-sequence reactive current component, besides regulatory GC-compliant positive-sequence reactive current injection. Last but not least, the proposed method replicates seamless functionality when alterations in irradiance and thus PV active power output occur during PCC faults.

Appendix

PV module parameters at STC:
V_{mpp}=49.78V, I_{mpp}=8.04A, P_{mpp}=400W, V_{oc}=60V, I_{sh}=8.56A, N_{cell}=96, α_i=0.043/°C, α_v=−0.367/°C, R_{sh}=389.9Ω, R_s=0.33Ω, A=1.02

DC-link and PCC located parameters of the plant:
DC-Link: C_{dc}=23mF, V_{dc}^{nom}=850V, $f_{sw_{PV-VSC}}$=5kHz
PCC: V=480V, f=50Hz, R_f=3$m\Omega$, L_f=0.1mH

Table I:
The entire values of the parameters, currents, voltages, and resulting powers of the simulation studies in this paper.

References

[1] K. Jia, J. Chen, G. Zhao, B. Yang, and T. Bi, "Second harmonic injection based recovery control of pv dc boosting integration system," *IEEE Trans. Smart Grid*, pp. 1022–1032, 2020.
[2] Energinet.dk, "Technical regulation 3.2.2 for pv power plants above 11 kw," *Tech. Rep. 14/17997-39*, 2016.
[3] S. Adhikari, F. Li, and H. Li, "P-q and p-v control of photovoltaic generators in distribution systems," *IEEE Trans. Smart Grid*, vol. 6, no. 6, pp. 2929–2941, 2015.
[4] M. Mirhosseini, J. Pou, and V. G. Agelidis, "Single- and two-stage inverter-based grid-connected photovoltaic power plants with ride-through capability under grid faults," *IEEE Trans. Sustain. Energy*, vol. 6, no. 3, pp. 1150–1159, 2015.
[5] A. Mojallal and S. Lotfifard, "Enhancement of grid connected pv arrays fault ride through and post fault recovery performance," *IEEE Trans. Smart Grid*, vol. 10, no. 1, pp. 546–555, 2019.
[6] A. Camacho, M. Castilla, J. Miret, L. G. d. Vicuña, and G. L. M. Andrés, "Control strategy for distribution generation inverters to maximize the voltage support in the lowest phase during voltage sags," *IEEE Trans. Ind. Electron.*, vol. 65, no. 3, pp. 2346–2355, 2018.
[7] J. Miret, M. Castilla, A. Camacho, L. G. d. Vicuña, and J. Matas, "Control scheme for photovoltaic three-phase inverters to minimize peak currents during unbalanced grid-voltage sags," *IEEE Trans. Power Electron.*, vol. 27, no. 10, pp. 4262–4271, 2012.
[8] A. Camacho, M. Castilla, J. Miret, L. G. d. Vicuña, and R. Guzman, "Positive and negative sequence control strategies to maximize the voltage support in resistive–inductive grids during grid faults," *IEEE Trans. Power Electron.*, vol. 33, no. 6, pp. 5362–5373, 2018.
[9] M. A. G. López, J. L. G. d. Vicuña, J. Miret, M. Castilla, and R. Guzmán, "Control strategy for grid-connected three-phase inverters during voltage sags to meet grid codes and to maximize power delivery capability," *IEEE Trans. Power Electron.*, vol. 33, no. 11, pp. 9360–9374, 2018.
[10] A. K. Gupta, M. S. Joshi, and V. Agarwal, "Improved transformerless grid-tied pv inverter effectively operating at twice the switching frequency with constant cmv and reactive power capability," *IEEE Trans. Emerg. Sel. Topics Power Electron.*, vol. 8, no. 4, pp. 3477–3486, 2019.
[11] M. Mirhosseini, J. Pou, and V. G. Agelidis, "Grid-connected photovoltaic power plant without phase angle synchronization able to address fault-ride-through capability," *IEEE Trans. Emerg. Sel. Topics Power Electron.*, vol. 8, no. 4, pp. 3467–3476, 2020.
[12] M. Nasiri and R. Mohammadi, "Peak current limitation for grid side inverter by limited active power in pmsg-based wind turbines during different grid faults," *IEEE Trans. Sustain. Energy*, vol. 8, no. 1, pp. 3–12, 2017.
[13] A. Q. Al-Shetwi, M. Z. Sujod, and F. Blaabjerg, "Low voltage ride-through capability control for single-stage inverter-based grid-connected photovoltaic power plant," *Solar Energy*, vol. 159, pp. 665–681, 2018.

TABLE I
PARAMETERS, CURRENTS, VOLTAGES, AND RESULTING POWERS OF THE ENTIRE SIMULATION STUDIES

Variable	Time Interval							
	A		B		C		D	
	Scenario 1	Scenario 2	Scenario 1	Scenario 2	Scenario 1	Scenario 2	Scenario 1	Scenario 2
$v_{df}^{+}(V)$	59	170	59	170	256	300	356	300
$v_{df}^{-}(V)$	0	-110	0	-110	0	-45	0	-45
α	1	1	1	1	0.621	0.329	0.621	0.329
m	0	0.65	0	0.65	0	0.15	0	0.15
γ	1	0.604	1	0.604	1	1	1	1
ζ	0	0	0	0	0.783	0.803	0.783	0.803
$i_{df-\lim}^{+}(kA)$	0	0	0	0	2.43	2.49	2.43	2.49
$i_{df}^{+}(kA)$	0	0	0	0	1.42	1.26	2.43	2.49
$i_{qf}^{+}(kA)$	3.1	1.874	3.1	1.874	1.926	1.02	1.926	1.02
$P_{0-\lim}(MW)$	0	0	0	0	0.93	1.096	0.93	1.096
$P_{grid}(MW)$	0	0	0	0	0.54	0.56	0.93	1.096
$P_{PV}(MW)$	0.06	0.05	0.06	0.05	0.57	0.574	0.992	1.143
$Q(MVAr)$	0.273	0.68	0.273	0.68	0.736	0.46	0.736	0.46

[14] K. Jia, C. Gu, Z. Xuan, L. Li, and Y. Lin, "Fault characteristics analysis and line protection design within a large-scale photovoltaic power plant," *IEEE Trans. Smart Grid*, vol. 9, no. 5, pp. 4099–4108, 2018.

[15] X. Liu, C. Li, M. Shahidehpour, Y. Gao, B. Zhou, Y. Zhang, J. Yi, and Y. Cao, "Fault current hierarchical limitation strategy for fault ride-through scheme of microgrid," *IEEE Trans. Smart Grid*, vol. 10, no. 6, pp. 6566–6579, 2019.

[16] M. Nasiri, J. Milimonfared, and S. H. Fathi, "A review of low-voltage ride-through enhancement methods for permanent magnet synchronous generator based wind turbines," *Renew. Sustain. Energy Rev.*, vol. 47, pp. 399–415, 2015.

[17] F. A. S. Neves, M. Carrasco, F. Mancilla-David, G. M. S. Azevedo, and V. S. Santos, "Unbalanced grid fault ride-through control for single-stage photovoltaic inverters," *IEEE Trans. Power Electron.*, vol. 31, no. 4, pp. 3338–3347, 2016.

[18] J. Miret, A. Camacho, M. Castilla, L. G. d. Vicuña, and J. Matas, "Control scheme with voltage support capability for distributed generation inverters under voltage sags," *IEEE Trans. Power Electron.*, vol. 28, no. 11, pp. 5252–5262, 2013.